Monte Carlo Simulations of Elastic Scattering with Applications to DC and High Power Pulsed Magnetron Sputtering for Ti_3SiC_2

Jürgen Geiser[1,*] and Sven Blankenburg[2]

[1] *Department of Mathematics, Humboldt-Universität zu Berlin, D-10099 Berlin, Germany.*
[2] *Department of Physics, Humboldt-Universität zu Berlin, D-10099 Berlin, Germany.*

Abstract. We simulate the particle transport in a thin film deposition process made by PVD (physical vapor deposition) and present several models for projectile and target collisions in order to compute the mean free path and the differential cross section (angular distribution of scattered projectiles) of the scattering process. A detailed description of collision models is of the highest importance in Monte Carlo simulations of high power impulse magnetron sputtering and DC sputtering. We derive an equation for the mean free path for arbitrary interactions (cross sections) that includes the relative velocity between the particles. We apply our results to two major interaction models: hard sphere interaction & screened Coulomb interaction. Both types of interaction separate DC sputtering from HIPIMS.

1 Introduction

The main reason for studying the collision processes of elastic scattering is the need for a reliable physical description of the interactions between ions and a plasma (background gas) in high power pulsed magnetron sputtering processes for the creation of uniform, stoichiometric thin films. MAX-phases experienced a renaissance in the mid 1990s, when

---

*Corresponding author. *Email addresses:* `geiser@mathematik.hu-berlin.de` (J. Geiser), `sven.blankenburg@physik.hu-berlin.de` (S. Blankenburg)

Barsoum synthesized relatively phase-pure samples of the MAX-phase Ti_3SiC_2, and discovered a material with a unique combination of metallic and ceramic properties: it exhibited high electrical and thermal conductivity, and it was extremely resistant to oxidation and thermal shock, and so is very attractive for industrial applications like proton exchange fuel cells (PEFC). These stoichiometries (MAX-phases) are described by the general formula $M_{n+1}AX_n$, where M is an early transition metal (Sc, Ti, V, Cr, Zr, Nb, Mo, Hf, Ta), A is an A-group element (Al, Si, P, S, Ga, Ge, As, Cd, In, Sn, Ti, Pb), and X is either Carbon and/or Nitrogen. The different MAX stoichiometries are often referred to as 211 ($n=1$), 312 ($n=2$). Recent developments have led to a new method of synthesizing thin films of MAX-phases on a substrate (workpiece): high power impulse magnetron sputtering (HIPIMS or HPPMS), see [1–4]. The most important ingredient in sputtering processes is a plasma, i.e., a partially ionized gas, which, at macroscopic scales, is electrically neutral. If a material body such as a substrate is immersed in a plasma it will acquire a potential slightly negative with respect to ground. This effect is known as a floating potential. The physical reason for this is the higher mobility of electrons than that of ions. Hence, more electrons reach the substrate surface than ions. A very sensitive quantity in sputtering processes (with respect to the experimental setup: gas-pressure, temperature, target-material, etc.) is the sputtering yield, which describes the ratio of atoms ejected from a target surface per incident ion. The sputtering yield can take almost any value from 0.1 up to 10. To optimize production, one is generally interested in obtaining values for the sputtering yield as high as possible. In order to obtain a well defined film stoichiometry at the substrate, one has to take into account the transport mechanism of the sputtered particles within the plasma. This can be done either within a macroscopic description of the transport phenomena, i.e., the solution of the advection–diffusion equation, or at a microscopic scale, via Monte Carlo simulations of the transport phenomena. This paper deals almost exclusively with the last approach, in the future, the ultimate goal of our work will be to link both approaches to each other (this will be presented in future papers).

This paper is organized as follows: In Section 2 we describe the concept of mean free path and derive, on the basis of the kinetic theory, an appropriate expression for the mean free path of an external particle (projectile) that is probing an ensemble of target particles that constitute an ideal gas (background gas). The main modification to standard mean free paths is to allow of initially moving targets. Section 3 studies, from first principles, the concept of differential cross sections. In Section 4 we present our Monte Carlo method based on a pathway model, see [5], and perform several simulations of direct current (DC) and high power pulsed magnetron sputtering (HIPIMS). At the end, in Section 5, we summarize our results and discuss perspectives for future work.

2 Collision model: mean free path

The mean free path or average distance between collisions for a gas molecule may be estimated from kinetic theory. If one assumes the gas consists of hard spheres (non over-

lapping spheres), then the effective collision area is given by

$$\sigma = \pi(d_1 + d_2)^2 = \pi D^2. \tag{2.1}$$

In time δt, the area sweeps out a volume of $V_{interaction}$ and the number of collisions can be estimated from the number of target molecules (n_V) that are in that volume

$$V_{interaction} = \sigma v \delta t. \tag{2.2}$$

The expression for the mean free path,

$$\lambda = \frac{|v_{proj}|\delta t}{V_{interaction} n_V} = \frac{|v_{proj}|\delta t}{\pi D^2 v \delta t n_V} = \frac{1}{\pi D^2 n_V}, \tag{2.3}$$

is a good approximation, but it suffers from a significant flaw—it assumes the target object's being at rest, which is of course nonsense, physically. We introducing the relative velocity between the gas objects

$$v_{rel} = \sqrt{2}v. \tag{2.4}$$

Here the $\sqrt{2}$ results from the molecular speed distribution of a mono atomic ideal gas (Maxwell–Boltzmann distribution). We therefore have the expression

$$\lambda = \frac{1}{\sqrt{2}\pi D^2 n_V}. \tag{2.5}$$

The number of molecules per unit volume can be determined from the state equation of the gas

$$pV = (1 + B_1 + B_2 + \cdots)RT. \tag{2.6}$$

If one assumes an ideal gas (non interacting and non overlapping gas particles) one can neglect the so called higher virial coefficients ($B_1 + B_2 + \cdots$). Inserting the state equation for an ideal gas into (2.5), one gets

$$\lambda = \frac{(1)RT}{\sqrt{2}\pi D^2 N_A p}. \tag{2.7}$$

Here R is the gas constant and N_A is Avogadro's number. This is an approximation for the mean free path of an atom/molecule of an ideal gas. In our problem, however, we have to calculate the mean free path of an external particle (projectile) which is not a member of the background gas (ideal gas). This can be done by modifying the average relative velocity between projectile and target. This is done in the next part.

2.1 The mean relative velocity between projectiles and targets

The background gas is assumed to be Maxwell distributed in velocity (this is motivated by the assumption of an ideal gas). Because the background particles are an ensemble (with statistically distributed velocities) one can just speak of a mean relative velocity $<|v_{rel}|>=<|v_{proj}-v_{target}|>$, which can be calculated via:

$$<|v_{rel}|>=\int\int\int_V |v_{proj}-v_{target}|Z(v_{target})dv_{target}, \tag{2.8}$$

where Z is the three-dimensional Maxwell distribution given by

$$Z(v_{target})=(A/\pi)^{3/2}\frac{1}{2\sqrt{2}}\exp(-Av_{target}^2), \tag{2.9}$$

with the abbreviation $A=M_{target}/2k_BT$. A complete derivation of the solution can be found in the Appendix. The result is

$$|v_{rel}|=\frac{\left[\left(s+\frac{1}{2s}\right)\mathrm{erf}(s)+\frac{1}{\sqrt{\pi}}\exp(-s^2)\right]}{3s}\times|v_{proj}|, \tag{2.10}$$

with $s=a\sqrt{A}$ (scalar) and $a=|v_{proj}|$. We now want to discuss a few special cases.

If the velocity of the projectile is very small, $|v_{proj}|\approx 0$, then $s\approx 0$ and therefore the following approximation holds

$$v_{rel}\approx v_{target}. \tag{2.11}$$

If the target objects are identical to the projectile objects (same mass and same mean velocity), then the following limit holds

$$|v_{rel}|\approx 1.41|v_{target}|, \tag{2.12}$$

which gives the factor $\sqrt{2}\approx 1.41$ and leads to the mean free path of an element of a mono atomic ideal gas (as expected). However, the general expression for the mean free path of a projectile probing into an ideal gas with pressure P_{gas} and temperature T is given by

$$\lambda_{proj}=\frac{3}{4\pi}\frac{s}{\left[\left(s+\frac{1}{2s}\right)\mathrm{erf}(s)+\frac{1}{\sqrt{\pi}}\exp(-s^2)\right]}\frac{k_BT}{\left(R_{ion}+R_{target}\right)^2 P_{gas}}. \tag{2.13}$$

There are a few things to say about this expression. First, the main assumption that the background gas (ensemble of target particles) is an ideal gas, is valid only within the high vacuum regime, i.e., small target density. Second, the interaction between the projectile and target atoms are assumed to be of hard sphere type, i.e., purely geometrical. If the projectile is a free particle between the interactions, its Hamilton function is

$$H=\frac{p^2}{2M_{proj}}=E. \tag{2.14}$$

In this case one can easily compute $a = |\boldsymbol{v_{proj}}| = \sqrt{2E/M_{proj.}}$. There follows immediately

$$s = a\sqrt{A} = \sqrt{\frac{E}{k_B T}}\sqrt{\frac{M_{target}}{M_{proj}}}. \tag{2.15}$$

In appropriate units (atomic units) the scalar s is

$$s = 107.7242\sqrt{\frac{E[eV]}{T[K]}}\sqrt{\frac{M_{target}}{M_{proj}}}. \tag{2.16}$$

Therefore the mean free path in units of cm is given by:

$$\lambda_{proj}[cm] = \frac{s}{\left[\left(s+\frac{1}{2s}\right)\mathrm{erf}(s)+\frac{1}{\sqrt{\pi}}\exp(-s^2)\right]} \cdot \frac{3.297\mathrm{cm}\cdot T[K]}{\left(R_{ion}[pm]+R_{target}[pm]\right)^2 P_{gas}[mbar]}. \tag{2.17}$$

In [2], a formula for the mean free path of ions surrounded by an ideal gas of pressure p_{ar} is used and given by

$$\lambda[cm] = \frac{4.39\mathrm{cm}\cdot T[K]}{\sqrt{\left(1+\frac{M_{ion}}{M_{target}}\right)}\left(r_{ion}[pm]+r_{target}[pm]\right)^2 p_{target}[mbar]}. \tag{2.18}$$

Table 1 shows the mean free path for ions at $E = 3$ eV and $T = 300$K and gas pressure $p = 4\times10^{-3}$ mbar.

Table 1: mean free paths for the different sputter species.

Ion	Eq. (2.17)	Eq. (2.18)
carbon (12)	12.96 cm	15.18 cm
silicon (28)	7.52 cm	7.71 cm
titanium (48)	5.03 cm	4.55 cm

In a sputtering process, the ions obey a kinetic energy distribution as well as an angular-distribution at the target. Because of different transport mechanisms, an ion loses to some extent its initial kinetic energy. The ions of a sputter process can therefore be classified into three groups. First, the *ballistic group*, such that any member of the ballistic group travels from the target to the substrate in a straight line because no collisions occur. The *transition group* is characterized by the observation that the path of the ion is not a straight line and therefore the ions of this group undergo some collisions but still retain some of their initial energy. The last group is the *thermalized* or *diffusive* group, where any member of this group has completely lost its initial kinetic energy. The motion of such an ion is therefore described by a random walk. The typical distances between the target and the substrate are of the order of 5–15 cm. Hence, at low argon pressures
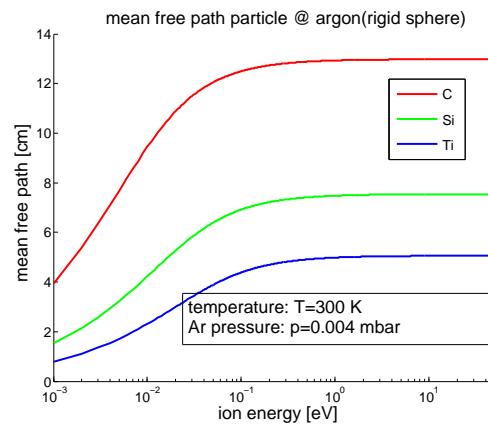
Figure 1: Mean free path of projectiles @ argon targets ($p = 4 \times 10^{-3}$ mbar and $T = 300$ K).

we can classify carbon as more or less ballistic, and silicon and titanium as transition or thermalized. One can also see that the formula used by [2] and [4] is quite a good approximation, although it lacks an energy dependency of the mean free path with respect to the ion energy. There have been several attempts to achieve an energy dependency of the mean free path. But most of them are more or less physical consistent. For example, in paper [6], a formula is used, whereby the energy dependency is obtained by modifying the naive mean free path by multiplying the naive formula by the ion energy. This is of course unphysical because it implies a zero mean free path at very low ion energies and consequently the associated cross section is infinite. We hope that our formula for the mean free path will be positively accepted within the community and might help implement a realistic description of the interactions between particles. In Fig. 1 one can see the results from Eqs. (2.16) and (2.17) with respect to the ion energy E (kinetic energy) at an argon pressure of $p = 4 \cdot 10^{-3}$ mbar and a constant temperature of $T = 300$ K, in which the following constants (see Table 2) were used.

Table 2: Atomic parameters for the different sputter species.

element	atomic mass [u]	atomic radius [pm]
Ar	39.948	71
C	12.0107	67
Si	28.0855	110
Ti	47.867	150

One can see that the mean free path increases with increasing kinetic energy of the ion and that the mean free path is almost constant (i.e., the classically obtained mean free path) at energies above 2 eV. The likelihood of ions to scatter off argon targets is not constant, because if the ions scatter off an target it loses some energy and therefore its mean free path becomes smaller. This iterative procedure continues. It is therefore of the

highest importance in situations in which one has to deal with multiple scattering, as is the case if the sputter-target and the substrate.

3 Collision model: Differential cross section & angular distribution

With the help of the mean free path λ one is able, within a Monte Carlo approach, to determine the collision frequency. But several questions are unanswered by a knowledge of the mean free path. If one is interested in a detailed description (kinematic) of the scattering process, one has to work out the differential cross section. We propose two descriptions; both are, within their limits, applicable. In the first model, we assume the target particle is initially at rest, whereas the second model will loosen this restriction.

3.1 Scattering with initially fixed targets

If the projectile velocity is much higher than the target velocity one can assume the target atoms are initially at rest. Describing the scattering process with the center of mass system (CMS) simplifies the calculations. The theoretical analysis of such a scattering process can be found in almost any text book on classical mechanics such as [7]. We use spherical coordinates, wherein θ, ϕ describes the coordinates in the laboratory and Θ, Φ are the coordinates in the CMS. The ratio

$$\rho = \frac{M_{proj}}{M_{target}} \frac{v_{t,1}}{v_{rel,1}} \tag{3.1}$$

can be used to connect the scattering angles in the laboratory and the CMS (radial symmetric scattering potential)

$$\cos\theta = \frac{\cos\Theta + \rho}{\sqrt{1 + 2\rho\cos\Theta + \rho^2}}. \tag{3.2}$$

The transformation from CMS coordinates to laboratory coordinates brings in the Jacobian as an extra factor:

$$\sigma(\theta) = \sigma(\Theta) \frac{\sin\Theta}{\sin\theta} \left| \frac{d(\Theta, \Phi)}{d(\theta, \phi)} \right|. \tag{3.3}$$

Because $\Phi = \phi$ the Jacobian reduces to

$$\sigma(\theta) = \sigma(\Theta) \left| \frac{d\cos\Theta}{d\cos\theta} \right|. \tag{3.4}$$

With the help of Eq. (3.2) one gets

$$\sigma(\theta) = \sigma(\Theta) \frac{\left(1 + 2\rho\cos\Theta + \rho^2\right)^{3/2}}{1 + \rho\cos\Theta}. \tag{3.5}$$

The energy transfer from projectile to target (elastic scattering) is given by:

$$\Delta E = \frac{E_{\text{proj,new}}}{E_{\text{proj,old}}} = \frac{1+2\rho\cos\Theta+\rho^2}{(1+\rho)^2}.$$

(3.6)

The differential cross section is however not exactly the scattering angle distribution, because we have to remember that the angular distribution is given by an extra factor of $\sin\theta$ followed by an integration over ϕ, i.e.,

$$\sigma_{total} = \int_0^\pi \underbrace{\int_0^{2\pi} \frac{\sin\theta\sigma(\theta)}{4\pi} d\phi}_{\text{probability distribution}} d\theta.$$

(3.7)

3.1.1　Hard sphere collision

In order to model the transport mechanism within a DC sputtering process, one recognizes experimentally that most of the background targets as well as the sputter particles are not ionized and therefore it seems absolutely reasonable that the interaction of both projectile and targets are purely geometrical and can be modeled by a hard sphere interaction. The scattering angle Θ_{CMS} in the center of mass system of a binary collision can in generally be calculated for any given interaction potential $V(r)$ with the help of

$$\Theta_{CMS} = \pi - 2\int_{r_0}^\infty (r\phi(r))^{-1} dr,$$

(3.8a)

$$\phi(r) = \left(\frac{r^2}{p^2} - 1 - \frac{r^2 V(r)}{1/2\mu v_{rel}^2 p^2}\right),$$

(3.8b)

where μ is the reduced mass in the CMS system, i.e., $\mu = (M_1 M_2)/(M_1+M_2)$ and v_{rel} is the relative velocity of the scattering partner. p is called the impact parameter. In Fig. 2 one can see the scattering angle θ in the laboratory of several incident projectiles at argon atoms (held at rest) and the maximal scattering angle θ_{max} in the laboratory with respect to the mass ratio ρ. In the case of a hard sphere potential, i.e.,

$$V(r) = \begin{cases} \infty, & \text{for } r < R, \\ 0, & \text{for } r \geq R, \end{cases}$$

(3.9)

the integral can be computed analytically and the result is

$$\Theta_{CMS} = 2\cos^{-1}(z).$$

(3.10)

Here we have used the dimensionless parameter $z = p/p_{max} = p/R$ with $R = R_1+R_2$ the radius of interaction. The impact parameter p is chosen to be uniformly distributed between 0 and p_{max}, i.e., $z \in U[0,1]$. In Fig. 2 one can see the results from single binary
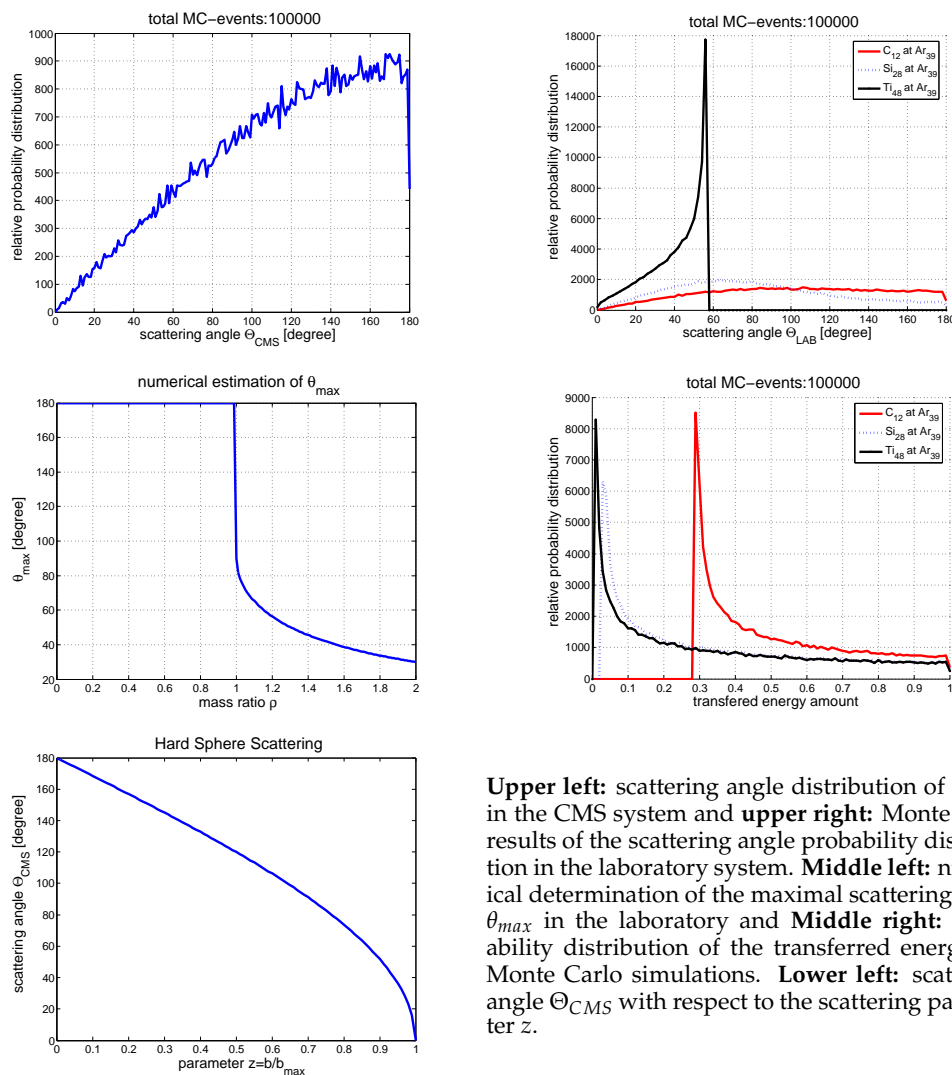
Figure 2: Results from one hard sphere collision (targets initially at rest).

Upper left: scattering angle distribution of Θ_{CMS} in the CMS system and **upper right:** Monte Carlo results of the scattering angle probability distribution in the laboratory system. **Middle left:** numerical determination of the maximal scattering angle θ_{max} in the laboratory and **Middle right:** probability distribution of the transferred energy via Monte Carlo simulations. **Lower left:** scattering angle Θ_{CMS} with respect to the scattering parameter z.

collisions for the sputter species C, Si, and Ti within the framework of hard sphere collisions. One can see that as long as the projectile mass is smaller than the target mass all scattering angles are allowed. However, this changes if the mass ratio becomes greater than 1. In this case only a cone of scattering directions is allowed, and the opening angle of the cone decreases with increasing mass ratio. In the case of titanium projectiles at argon targets, only scattering angles between 0 and $\theta_{max} \approx 60$ degrees are allowed. Titanium projectiles are therefore subjected to forward scattering and the cone angle is around 120 degrees. The above approach is quite satisfactory if one assumes highly energetic projectiles (with respect to target velocity) and the suppression of multi-scattering events. A

proper description of the kinematics should include the random motion of the target projectiles and therefore an energy dependency for the differential cross section. The total cross section has to be unchanged, because the total area per target cannot depend on the relative velocity of the target and projectile, because the total cross section is an intrinsic quantity.

3.1.2 Screened Coulomb collision

Now we want to investigate the kinematics of the scattering process where we assume a Coulomb-like interaction between the sputter particles and the gas atoms (again neglecting interactions between the sputter particles). This is motivated by the experimentally observed fact that in high power impulse magnetron sputtering processes, a fraction of the background gas as well as the sputtered particles are ionized and consequently the interaction model should include long range interactions due to electrical repulsion between both particles (ions). Our method of investigation is quite the same as in the previous (hard sphere) collision model. First we will specify the interaction potential and after that we compute the scattering angle in the CMS system. With the help of the scattering angle in the CMS we can compute the scattering angle in the LAB frame and also the energy loss. We have chosen the following screened interaction potential:

$$V(r) = \frac{Z_1 Z_2 k}{r} \exp(-r/a). \tag{3.11}$$

Here Z_1 and Z_2 are the atomic numbers of the collision partners, r is the radial distance between both partners, k is a constant ($k = 1.44 \text{MeV fm}$) and a is the screening length given by

$$a = \frac{a_0}{\sqrt{\left(\sqrt{Z_1} + \sqrt{Z_2}\right)}}, \tag{3.12}$$

$a_0 = 0.53 \cdot 10^{-10} m$ being the first Bohr radius of the hydrogen atom. For any given scattering potential, the scattering angle in the CMS system can be computed with the help of Eq. (3.8). As we mentioned earlier, the integral can be solved analytically in the situation of a hard sphere interaction and a pure Coulomb interaction. However, we have chosen a screened Coulomb potential and we must therefore evaluate the integral numerically. In order to reduce round-off errors, we reformulate the integral (this procedure is motivated by [8]):

$$\Theta_{CMS} = 2 \text{Arccot} \left(\frac{2\chi_2}{\exp(-1/z_0)} \right) + 2\chi_0\chi_2 \int_0^{z_0} \left(y_0^{1/2}(z) - y^{1/2}(z) \right) dz. \tag{3.13}$$

Here we made use of

$$\chi_0 := \frac{b}{a} = \frac{Z_1 Z_2 \sqrt{\left(\sqrt{Z_1} + \sqrt{Z_2}\right)}}{E_{CMS}[\text{eV}]} \cdot 27.17, \tag{3.14a}$$

$$\chi_2 := \frac{p}{b} = \frac{p[10^{-10}\text{m}]E_{CMS}[\text{eV}]}{Z_1 Z_2} \cdot \frac{1}{14.4}, \tag{3.14b}$$

$$E_{CMS} = \frac{\left((1+1/2s)\text{erf}(s) + 1/\sqrt{\pi}\exp\left(-s^2\right)\right)^2}{\left(1 + \frac{M_{proj}}{M_{target}}\right)9s^2} \cdot E_{proj}, \tag{3.14c}$$

$$y_0(z) = 1 - (\chi_0\chi_2)^2 z^2 - \chi_0 z \exp(-1/z_0), \tag{3.14d}$$

$$y(z) = 1 - (\chi_0\chi_2)^2 z^2 - \chi_0 z \exp(-1/z), \quad z = r/a. \tag{3.14e}$$

Our procedure is then as follows: for a given impact parameter p in units of fm we can solve the integral numerically for every sputtering species. Because this is very time consuming we have done this for several impact parameters and every species before the simulation and we have stored the results in a data file which is then used during the simulation. During the Monte Carlo simulation an impact parameter is chosen from a uniform distribution between zero and p_{max} whereby we have chosen $p_{max} = 4 \cdot 10^{-10}$ m, because for an impact parameter greater than p_{max} the scattering angle in the laboratory system is in general smaller than 0.1 degree. With the help of the numerical integration of Eq. (3.8) we can compute the scattering angle in the CMS and therefor compute the scattering angle in the laboratory system. Recall, that here we choose the impact parameter to be uniformly distributed in the CMS system and not the scattering angle (as we did in the hard sphere scattering). Recall also that we have chosen an appropriate relative velocity between projectiles and targets (the derivation can be found in the Appendix). In Fig. 3 one can see the scattering angle of several species with respect to a screened Coulomb interaction potential. Again, all scattering angles between zero and 180 degree
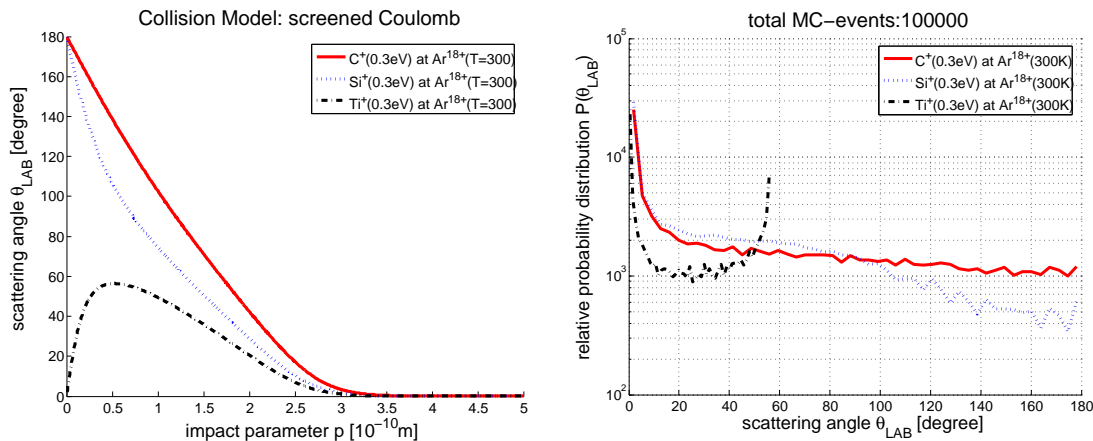
Left: scattering angle θ_{LAB} with respect to the impact parameter and **right:** the relative scattering angle distribution of Θ_{LAB}.

Figure 3: Results from the screened Coulomb collision model under the assumption of fully ionized argon gas particles and simply ionized projectile particles.

are possible for projectiles with a mass smaller than the target mass. For projectiles with a mass greater than the target mass there exists a maximum scattering angle and therefore the scattering occurs only with an scattering cone of finite opening angle, i.e., forward scattering in the laboratory system will be preferred for titanium. In Fig. 3 one can see the functional dependency of the scattering angle in the laboratory stem with respect to the impact parameter as well as the relative probability distribution of the scattering angle θ_{LAB} in the laboratory system.

4 Monte Carlo simulations

In Fig. 4 one can see the geometry of the simulated sputter-deposition chamber.

4.1 Sputtering from target

Sputtering from a circular planar magnetron causes the formation of a race-track in the target (see Fig. 4). The profile of the race-track is approximated by a Gauss distribution:

$$P(R) = \frac{1}{\sigma\sqrt{2\pi}}\exp\left(-\frac{R-\mu}{2\sigma^2}\right).$$

The radius of the experimental race-track is 7.5 mm (which is used for the mean μ of the Gauss distribution) and the width of the race-track is 5 mm (from which the standard deviation is calculated to be $3\sigma = 2.5$ mm).
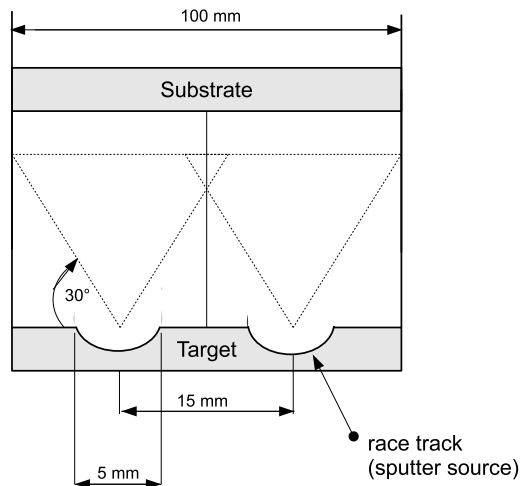
Figure 4: The chosen geometry of the simulated sputter-deposition chamber.

Table 3: Input parameter used to simulate the sputtering process from the compound target.

atom	lattice binding energy [12] [eV]	surface binding energy [eV]
carbon	281	0.5
silicon	99	0.5
titanium	485	0.5

4.2 Angular distribution

The initial distributions of out-coming particles from the sputter material is obtained by using the TRIM Monte Carlo code [10]. We used the latest version of the code (TRIM 2008) in order to obtain the initial angular distribution of the sputtered particles, the sputtering yields, as well as the energy distribution. We modeled our compound target as a one layer material with specific parameters given in Table 3. To have more a realistic angular distribution of the light elements (e.g. C (carbon)), we have also taken into account the dynamic variations in the surface composition. We compared the results with TRIDYN (dynamic TRIM), based on the low concentration of C, and did not see any different results with carbon. It should be stated, that studies on comparison the results with TRIDYN are done in [11], where they obtain differences in the angular distributions of carbon.

For the sputtering process we used a beam of monoenergetic argon ions approaching the target perpendicularly to its surface with an energy of 500 eV. Because of the relatively low energy of the argon atoms the sputtering process is a surface process.

4.3 Ionization rates and ion energy distribution

The ionization rates of sputtered particles are very low, and thus no influence on the particle distribution is assumed. But in contrast, the particle's energy seems to be of high importance. Unfortunately, until now no experimentally obtained energy distribution for our compound target (Ti_3SiC_2) is available. We therefore used the TRIM-code in order to set up the initial conditions at the sputter target. In Fig. 5 one can see the ion energy distribution, which is obtained by TRIM. One can see that most of the ions are at energies close to 3 eV. In order to simulate the ion transport it is necessary to calculate the velocity of the ions. From

$$E = H = \frac{p^2}{2M} = \frac{1}{2}Mv^2,$$

it follows that

$$v = \sqrt{\frac{2E}{M}}. \tag{4.1}$$

The energy of the ions is given in units of electron volts (eV) and the mass of the ions is given in atomic units (u). Therefore one can compute the velocity in units of cm per
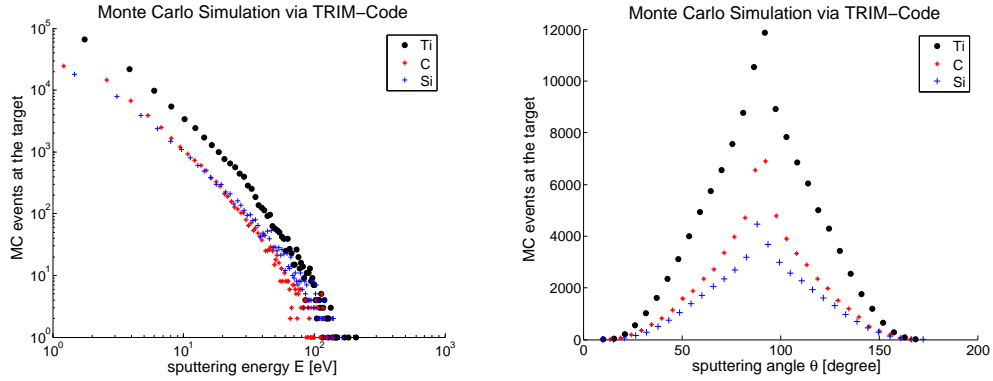
Figure 5: Simulated energy and angular distribution of the sputtered species at the target by using the TRIM-code. One can see that most of the sputter particles have energies around 3–5 eV. The angular distribution is an over-sine distribution. Here we used a monoenergetic beam of argon ions impacting perpendicularly to the target surface with an energy of 500 eV and constant surface binding energies of the sputtered particles of 0.5 eV.

second by using

$$v = \sqrt{\frac{2E[eV]}{m[u]}} \cdot 9.824 \cdot 10^5 = v[cm/s]. \tag{4.2}$$

In two spatial dimensions, one has two velocity components. ϕ_0 is the direction angle of the ion (see angular distribution of the ions) and the velocity components can be calculated by

$$v_x = v \cdot \cos(\phi_0), \tag{4.3}$$
$$v_y = v \cdot \sin(\phi_0). \tag{4.4}$$

Now, we want to apply our two interaction models to DC and high power impulse sputtering for Ti_3SiC_2. In general if several independent interaction mechanism can occur, the mean free path is not an additive quantity, but in contrast the total cross section is an additive quantity. In order to reduce the computational effort, we decided to use an event-driven Monte Carlo method in contrast to the usually used time-driven Monte Carlo method. It is therefore necessary to determine when the next interaction will occur. If the velocity (v) and the mean free path (λ) of the particle are known, one can compute the collision frequency τ by using

$$\tau = \frac{v}{\lambda} = \frac{\sqrt{v_x^2 + v_y^2}}{\lambda}. \tag{4.5}$$

With the help of the collision frequency one is able to compute the time interval until the interaction occurs

$$\delta t = -\frac{\log(r)}{\tau}. \tag{4.6}$$
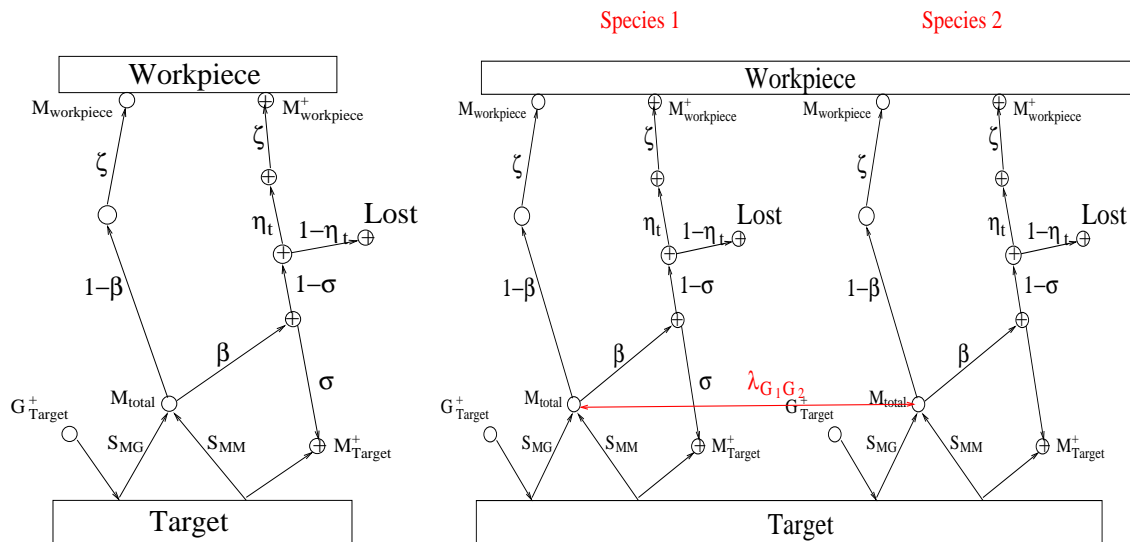
Figure 6: **Left:** Single pathway model and **right:** Multi pathway model (Christie 2005).

Here r is a random number from a uniform distribution between zero and one. Instead of simulating the trajectory of all particles in a Monte Carlo run with a fixed time step, one can use the above mentioned formula to adjust the time step. The strategy is as follows: one calculates the time interval δt for every particle (except the background particles) within a Monte Carlo run (trial), and finds the minimum value. The particle related to the minimum value of δt will first undergo an interaction. The Monte Carlo time step is set to this minimum value (this makes it an event driven MC). After the time step, the specific particle will undergo the interaction, and all other particles just move along their specific trajectory, i.e., in the absence of any external forces the trajectory is just a straight line (this is motivated by the fact the even if external fields are set up, inside the plasma the particles will behave as if they were free, due to the electric conductance of the plasma). If an interaction with the background gas (argon) occurs, we assume a uniform impact parameter distribution in the center of mass system (CMS) between the ion and the background gas. We first describe the simulations of DC sputtering; thereafter the simulations concern high power impulse magnetron sputtering. The several interaction processes can be put into an abstract interaction model (the pathway model, see [5]) that binds the interaction parameters together. A schematic drawing can been seen in Fig. 6.

4.4   DC sputtering

In DC sputtering with low direct currents one can use the elastic hard sphere interaction to model the transport phenomena at the microscopic scale.

Table 4: Experimental setup parameter concerning the first experiment.

Parameter	Value
Temperature (T)	300 K
Ar-pressure (p_{Ar})	$4 \cdot 10^{-3}$ mbar
S-T-distance (d)	variable from 1 cm to 24 cm

Table 5: Experimental setup concerning the second experiment.

Parameter	Value
Temperature (T)	300 K
Ar-pressure (p_{Ar})	$4 \cdot 10^{-3}$ mbar
S–T distance (d)	variable from 1 cm to 24 cm

4.4.1 First experiment: Only hard sphere interaction

In Fig. 7 the results of 100,000 Monte Carlo events are shown, in which we used the experimental setup parameters in Table 4.

4.5 High power impulse magnetron sputtering

In HIPIMS one can assume that at least a fraction of particles (sputter particles as well as target particles) are ionized. Unfortunately, there is no specific relation between pulse duration and/or pulse height and the percentage of ionized particles. The next results are therefore very academic. In our first experiment concerning HIPIMS we assume that all gas particles and sputter particles are simply ionized. This is of course a realistic property for the gas particles (argon) but not for the sputter particles.

4.5.1 Second experiment: Only Coulomb interaction

If one assumes all sputter particles and all gas particles are at least simply ionized, then the interaction is completely described by the Coulomb or screened Coulomb interaction. For sake of simplicity, we assume only simply ionized particles. The results from Monte Carlo simulations can be seen in Fig. 8 whereby we used the experimental setup parameters in Table 5.

4.5.2 Third experiment: Mixed interactions

If one assumes the sputter particles consist of ionized as well as neutral atoms two interactions with the background gas can occur: hard sphere collisions if one of the collision particles is neutral, and Coulomb interactions if both collision particles are at least simply ionized. We assume the particles are only simply ionized and therefore we have chosen the following (see Table 6) effective atomic numbers Z_{eff} with respect to the Slater rules in atomic physics.
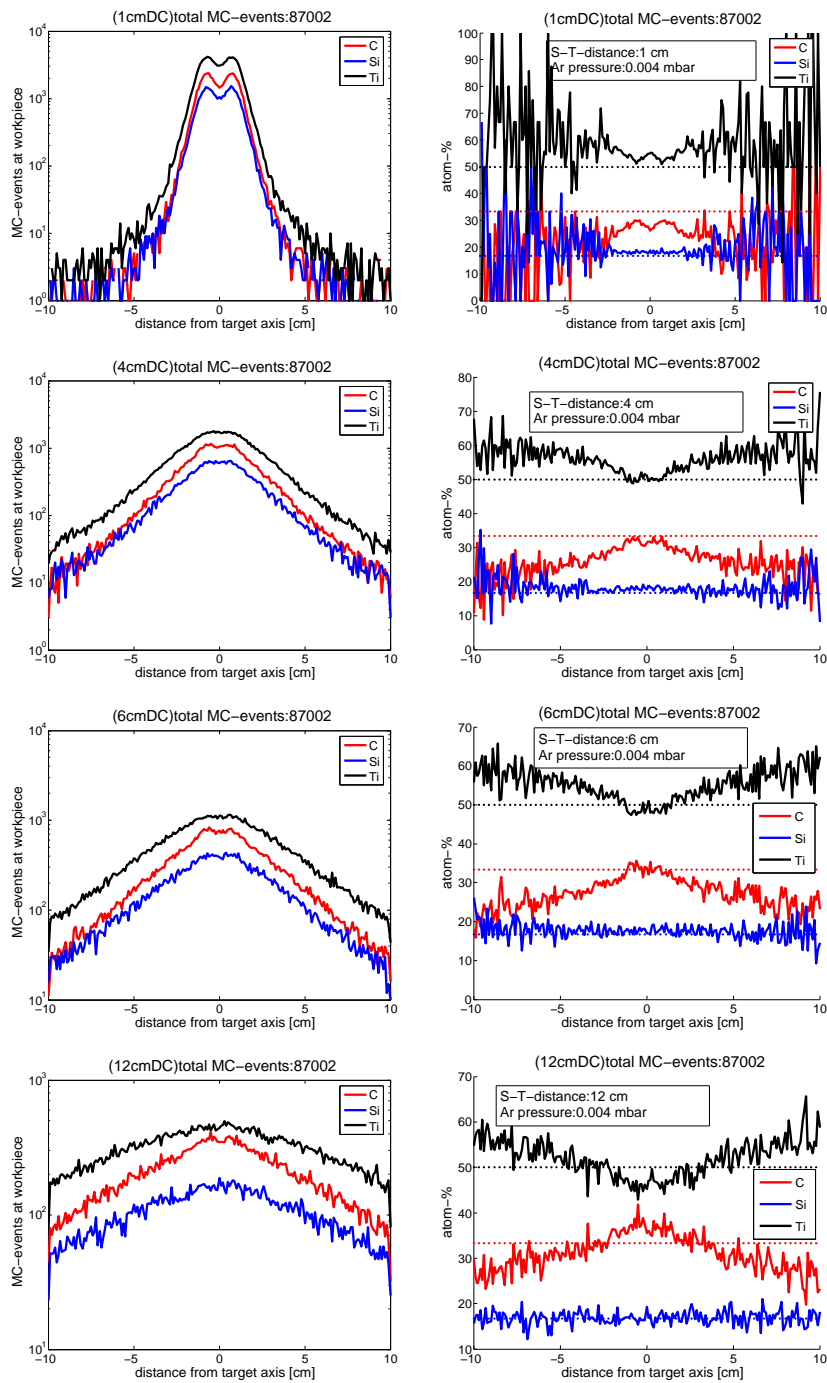
Left: registered Monte Carlo events at the workpiece and **right:** stoichiometric composition at the workpiece for several target–substrate distances in cm in which we assumed a pure hard sphere interaction between the sputter particles and the gas particles.

Figure 7: Results from the first experiment.
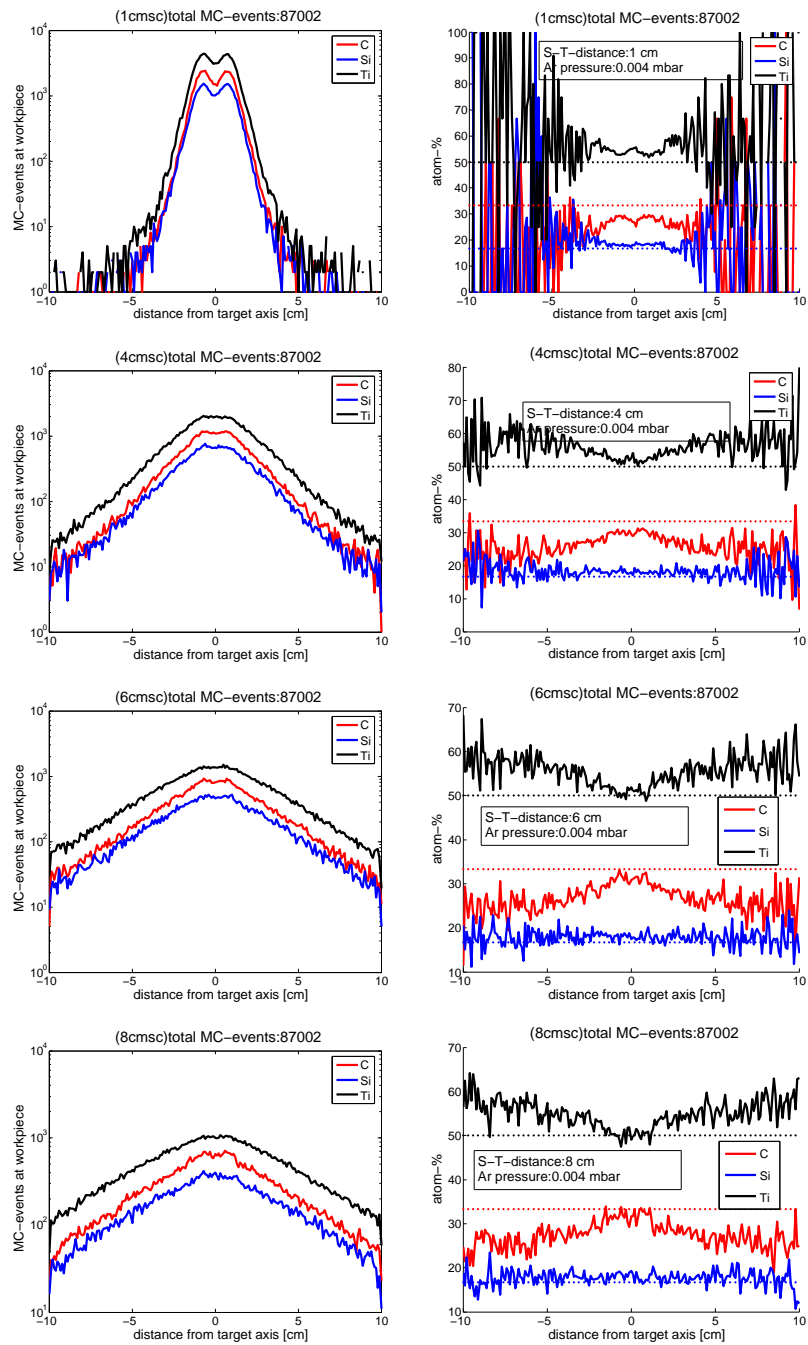
Left: Registered Monte Carlo events at the workpiece and **right:** stoichiometric film composition at the workpiece for several target–substrate distances in cm in which we assumed a pure Coulomb interaction between the sputter particles and the gas particles (simple ionized species). One can easily see the effect of the two sputter sources on the stoichiometric film composition at small substrate–target distances. This effect smears out at far distances.

Figure 8: Results from the second experiment.

Table 6: Calculated effective atomic numbers by using the Slater rules.

atom (ionized)	electron configuration	Z_{eff}
$_6C^+$	$(1s^2),(2s^22p^1)$	$6-2.75=3.25$
$_{14}Si^+$	$(1s^2),(2s^22p^6)(3s^23p^1)$	$14-9.85=4.15$
$_{22}Ti^+$	$(1s^2),(2s^22p^6),(3s^23p^63d^1),(4s^2)$	$22-19=3$
$_{18}Ar^+$	$(1s^2),(2s^22p^6),(3s^23p^5)$	$18-11.25=6.75$

Table 7: Experimental setup according the third experiment.

Parameter	Value
Temperature (T)	300 K
Ar-pressure (p_{Ar})	$4 \cdot 10^{-3}$ mbar
S-T-distance (d)	constant 5 cm
percentage of ionized carbon	30% (5–10 %)
percentage of ionized silicon	30% (20–30 %)
percentage of ionized titanium	30% (50–90 %)
percentage of ionized argon	variable from 0% up to 100%

In Fig. 9 one can see the results from our simulation in which we used the following (see Table 7) experimental setup parameters, (we do not have to much difference between the higher ionizations).

The results from the Monte Carlo simulation with several ionization degrees of argon atoms indicates that the ionization degree plays almost no role for our experimental setup parameter. All results show a dominance of titanium atoms at far distances from the target axis at the substrate. The most reliable member of the stoichiometry is again silicon. One can easily see that the effect of the ionization degree of argon atoms is suppressed due to the low ionization degree of the sputter particles. There are several experimentally obtained indications that the ionization degree of the sputter particles is not the assumed one, but particle dependent (electronic structure) as well as particle energy dependent. Therefore, further investigations concerning the ionization degree of the sputtered particles as well as the argon atoms are important and will be the subject of future paper.

4.5.3 Link to the pathway model & convergence test

In the following section we want to investigate the link with the pathway model [5] and our Monte Carlo simulations. The most important parameter in the pathway model of the transport phenomena is the loss factor. First predictions (rough estimations) can be made by inspection of the mean free paths for the sputter species. Carbon has almost the largest mean free path and therefore it will be just slightly affected by the interaction mechanism with the background gas. In Fig. 10 one can see our results for the loss factor of several sputter species and the different interaction models, i.e., pure hard sphere and
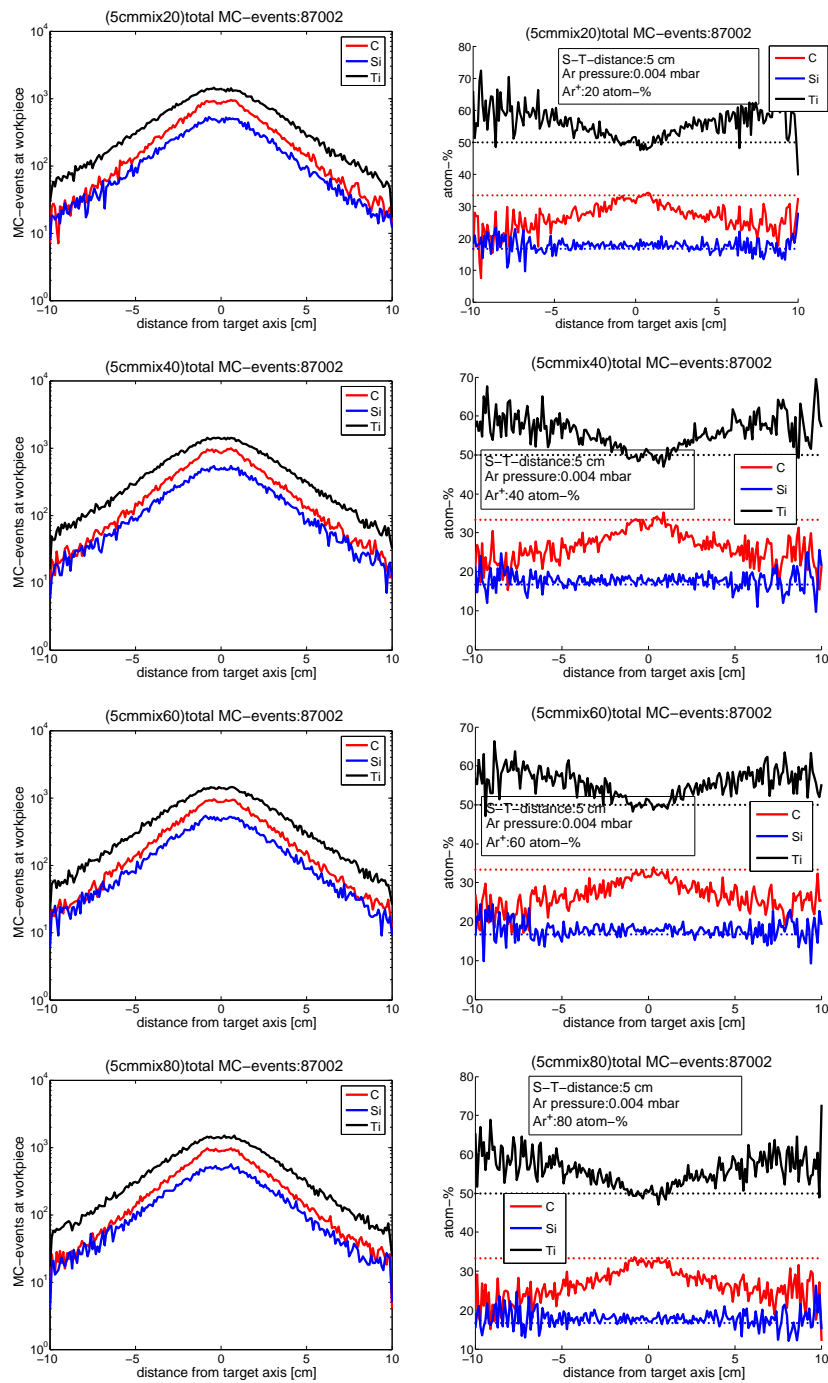
Left: registered Monte Carlo events at the workpiece and **right:** stoichiometric composition at the workpiece for several ionization degrees of argon in which we respected mixed interactions between the sputter particles and the gas particles (simple ionized species).

Figure 9: Results from the third experiment.
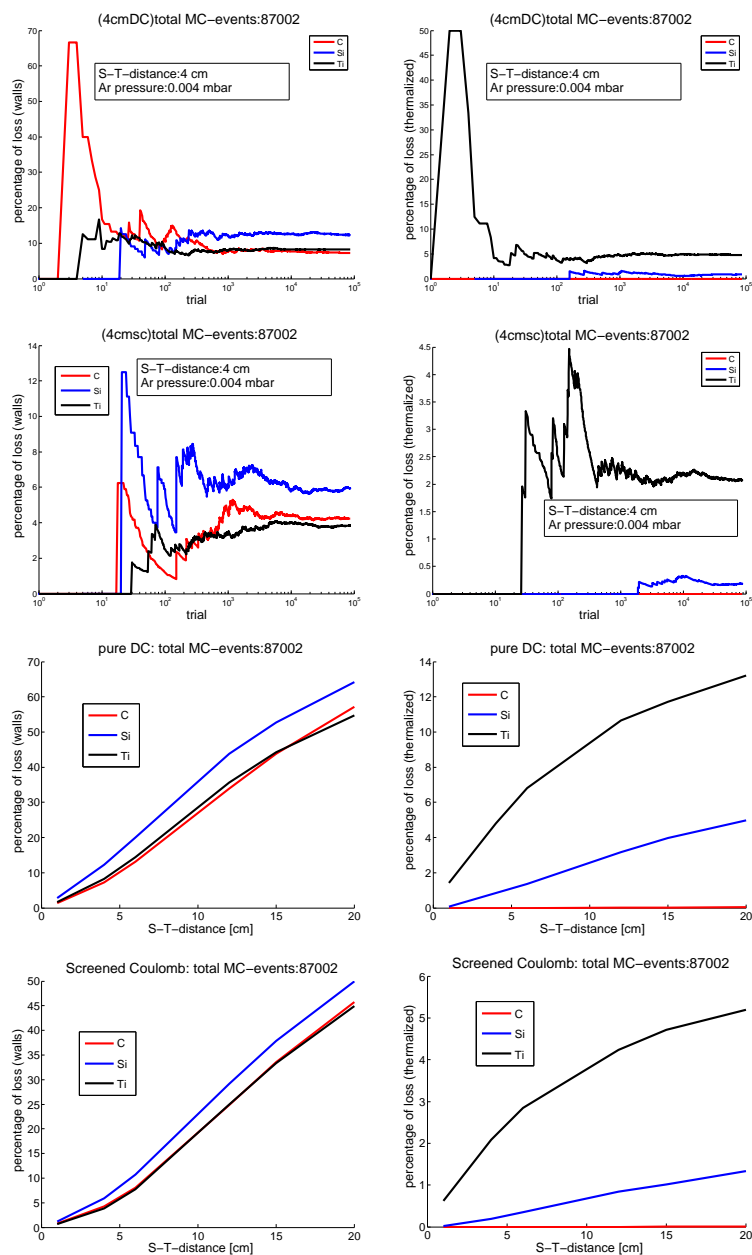
First row left: Loss factor due to interaction with walls for pure hard sphere interaction and **first row right:** Loss factor due to thermalization. **Second row left:** Loss factor due to interaction with walls for pure screened Coulomb interaction and **second row right:** Loss factor due to thermalization. **Third row left:** Loss factor due to interaction with walls for pure hard sphere interaction and **third row right:** Loss factor due to thermalization with respect to the substrate–target distance (S–T distance). **Fourth row left:** Loss factor due to interaction with walls for pure screened Coulomb interaction and **fourth row right:** Loss factor due to thermalization with respect to the substrate–target distance (S–T distance).

Figure 10: Link to the pathway model (loss factor).

pure screened Coulomb (described by the first two experiments). One can easily see that the values for the loss factor are almost constant after some equilibrium trials. This indicates a way of observing the convergence behavior of our Monte Carlo algorithm. Thus, with the help of the loss factor we can estimate the minimum Monte Carlo trials within a simulation and conclude from the equilibrium tendency that our implementation was done correctly. It is important to remember that the equilibrium MC time (number of MC trials) for the loss factor differs from Monte Carlo run to Monte Carlo run even with the same experimental setup parameter. We see that 50,000 Monte Carlo trials (events) are almost enough to equilibrate the system, i.e., reach convergence. One can also see the sensitivity of the loss factor with respect to different interaction mechanism between target atoms and projectiles. The loss factor for Coulomb interactions in general is smaller than the loss factor for hard sphere interactions.

5   Conclusion

So far, we have developed an appropriate Monte Carlo method based on a pathway model for interactions between sputtered particles and a background gas, assumed to be an ideal gas. We have set up a novel equation for the mean free path which incorporates all physical parameter such as temperature and gas pressure, but most importantly it respects the movement of the target atoms, i.e., the argon particles. With the help of our theoretical investigations we performed several Monte Carlo simulations for direct current (DC) and high power impulse magnetron sputtering (HIPIMS). The results from our simulations are qualitatively in agreement with experimentally obtained film compositions at the substrate as in the target composition. We were thus able to show that in DC sputtering the main interaction between the sputter particles and the background gas is of hard sphere type, i.e., purely geometrical. In HIPIMS a mixture of hard sphere and Coulomb interaction takes place. Unfortunately, the lack of experimentally obtained data concerning the ionization degree of the sputtered particles and the background gas forbids a direct comparison between simulation and experiments. In the future we hope to extract the ionization degree from first principles or by data fitting to experimentally obtained results. The effect of moving targets on the differential cross section, i.e., the angular distribution of sputtered particles, cannot be neglected. The effect of initially moving targets (with respect to the Maxwell velocity distribution) is especially important within the thermal group, i.e., with an energy ratio of the target and projectile of about one. Carbon and silicon are almost not members of the thermal group (because of their large mean free path). But titanium is a member of the thermal or diffusive group. In the case of a pure hard sphere interaction between argon and titanium, almost all scattering angles in the laboratory system can occur (in contrast to the initially resting target approach). The calculation and implementation of the initially moving target approach is in progress and includes an appropriate Monte Carlo Markov chain method.

Acknowledgments

Appendix: Derivation of the mean relative velocity

Within the framework of statistical mechanics, the mean value of an observable O can be computed via

$$<O> = \frac{\int\int O(q,p)Z(q,p;H)\,d^{3N}q\,d^{3N}p}{\int\int p Z(q,p;H)\,d^{3N}q\,d^{3N}p}. \tag{A.1}$$

With q the canonical coordinates and p the canonical momenta of an N-particle system, i.e., with Hamiltonian $H(q,p)$ and obeying Hamiltonian's equations of motion. The probability distribution Z depends on the total Hamiltonian H of the system. Within the canonical ensemble one has the following relation

$$Z = \exp\left(-\frac{H(q,p)}{k_B T}\right). \tag{A.2}$$

With $p = mv$ and the assumption of an ideal gas, the Hamilton function for the background gas is constructed by means of the kinetic energies of the gas particles

$$H = \sum_{i=1}^{N} \frac{p_i^2}{2m_i}. \tag{A.3}$$

If $O = O(p)$ then the coordinate integration gives a volume factor in the numerator and denominator and therefore no contribution. The momentum integration can be done immediately and results in Gaussian integrals. The result for the mean relative velocity is therefore given by

$$<O = v_{rel}> = \int\int\int_V |v_{proj} - v_{target}|\widetilde{Z}(v_{target})\,dv_{target}, \tag{A.4}$$

with $\widetilde{Z} = (A/\pi)^{3/2}\frac{1}{2\sqrt{2}}\exp(-Av^2)$ the reduced partition function (Maxwell distribution) and $A = M_{target}/2k_B T$. By substituting $\boldsymbol{u} = \boldsymbol{v_{target}} - \boldsymbol{v_{proj}}$ and $d\boldsymbol{u} = \boldsymbol{v_{target}}$ one gets

$$<|\boldsymbol{v_{rel}}|> = \int\int\int_V |\boldsymbol{u}|\exp\left(-Av_{proj}^2 - 2Av_{proj}u - Au^2\right)d\boldsymbol{u}$$

$$= \underbrace{\frac{(A/\pi)^{3/2}\exp\left(-Av_{proj}^2\right)}{2\sqrt{2}}}_{=:C(a,A)}\int\int\int_V |\boldsymbol{u}|\exp\left(-2Av_{proj}\boldsymbol{u} - Au^2\right)d\boldsymbol{u}. \tag{A.5}$$

By using spherical coordinates with $r=|\boldsymbol{u}|$, $a=|\boldsymbol{v}_{proj.}|$ and $\boldsymbol{v}_{proj}\cdot\boldsymbol{u}=|\boldsymbol{v}_{proj}|\cdot|\boldsymbol{u}|\cos\theta$ one gets

$$
\begin{aligned}
<|\boldsymbol{v}_{rel}|> &= C(a,A)\int_0^\infty\int_0^{2\pi}\int_0^\pi r\exp\left(-Ar^2-2A\cdot a\cdot r\cdot\cos\theta\right)r^2\sin\theta\,d\theta\,d\phi\,dr \\
&= 2\pi C(a,A)\int_0^\infty r^3\int_0^\pi\exp\left(-Ar^2-2Aar\cos\theta\right)\sin\theta\,d\theta\,dr.
\end{aligned}
\tag{A.6}
$$

The double integral on the right hand side can be evaluated and its solution is

$$
\begin{aligned}
&\int_0^\infty r^3\int_0^\pi\exp\left(-Ar^2-2Aar\cos\theta\right)\sin\theta\,d\theta\,dr \\
&= \frac{\left(\frac{A}{\pi}\right)^{3/2}\exp\left(-a^2A\right)}{2\sqrt{2}}\left(\frac{2\sqrt{A}a+(2Aa^2+1)\exp\left(a^2A\right)\sqrt{\pi}\,\mathrm{erf}\left(a\sqrt{A}\right)}{4aA^{5/2}}\right).
\end{aligned}
\tag{A.7}
$$

After some simplification the mean relative velocity is

$$
<|\boldsymbol{v}_{rel}|> = \frac{\left(2a+\frac{1}{Aa}\right)\mathrm{erf}\left(a\sqrt{A}\right)+\frac{2\exp\left(-a^2A\right)}{\sqrt{A}\sqrt{\pi}}}{4\sqrt{2}}.
\tag{A.8}
$$

Here we made use of the scalar $s:=a\sqrt{A}$.

With $a=|\boldsymbol{v}_{proj}|$ the final result for the mean relative velocity between projectiles probing into a mono-atomic ideal gas is given by

$$
<|\boldsymbol{v}_{rel}|> = \frac{\left[\left(s+\frac{1}{2s}\right)\mathrm{erf}(s)+\frac{1}{\sqrt{\pi}}\exp\left(-s^2\right)\right]}{3s}\times|\boldsymbol{v}_{proj}|.
\tag{A.9}
$$

References

[1] J. Alami, P. Eklund, J. Emmerlich, O. Wilhelmsson, U. Jansson, H. Hogberg, L. Hultman, and U. Helmersson, High-power impulse magnetron sputtering of Ti-Si-C thin films from a Ti3SiC2 compound target, Thin Solid Films 515 (2006), 1731-1736.

[2] P. Eklund, M. Beckers, U. Jansson, H. Hogberg, and L. Hultman, The $M_{n+1}AX_n$ phases: Materials science and thin-film processing, Thin Solid Films 518 (2010), 1851-1878.

[3] P. Eklund, M. Beckers, J. Frodelius, H. Hogberg, and L. Hultman, Magnetron sputtering of Ti3SiC2 thin films from a compound target, J. Vac. Sci. Technol. A 25 (2007), 1381–1388.

[4] K. Sarakinos, J. Alami, and S. Konstantinidis, High power pulsed magnetron sputtering: A review on scientific and engineering state of the art, Surf. Coat. Tech. 204 (2010), 1661-1684.

[5] D.J. Christie, Target material pathways model for high power pulsed magnetron sputtering, J. Vac. Sci. Technol. 23 (2005), 330–335.

[6] S. Mahiheu, G. Buyle, D. Depla, S. Heirwegh, P. Ghekiere, and R. De Gryse, Monte Carlo simulation of the transport of atoms in DC magnetron sputtering, Nucl. Instrum. Methods Phys. Res. B 243 (2006), 313–319.

 [7] H. Goldstein, Classical Mechanics, 2nd edition, Addison-Wesley: Reading, MA, USA, 1980.
 [8] E. Everhart, G. Stone, and R.J. Carbone, Classical calculation of differential cross section for scattering from a Coulomb potential with exponential screening, Phys. Rev. 99 (1955), 1287–1290.
 [9] A. Russek, Effect of target gas temperature on the scattering cross section, Phys. Rev. 120 (1960), 1536–1542.
[10] J.P. Biersack and W. Eckstein, Sputtering studies with the Monte Carlo Program TRIM.SP, Appl. Phys. A 34 (1984), 73–94.
[11] J. Neidhardt, S. Mraz, J.M. Schneider, E. Strub, W. Bohne, J. Röhrich, and C. Mitterer, Experiment and simulation of the compositional evolution of TiB thin films deposited by sputtering of a compound target, J. Appl. Phys. 104 (2008), 063304.
[12] D.P. Riley, D.J. O'Connor, P. Dastoor, N. Brack, and P.J. Pigram, Comparative analysis of Ti3SiC2 and associated compounds using x-ray diffraction and x-ray photoelectron spectroscopy, J. Phys. D: Appl. Phys. 35 (2002), 1603-1611.